JOURNAL OF MATERIALS SCIENCE **37** (2002) 4063–4071

# Oxidation behavior of *in situ* TiB short fibre reinforced Ti-6Al-1.2B alloy in air

ERLIN ZHANG*
*National Key Laboratory for Precision Hot -processing of Metal, Harbin Institute of Technology, Harbin 150001, People's Republic of China*
*E-mail: Erlin.Zhang@brunel.ac.uk*

GANG ZENG, SONGYAN ZENG
*School of Materials Science and Engineering, Harbin Institute of Technology, Harbin 150001, People's Republic of China*

The oxidation behavior of an *in situ* TiB short fibre reinforced Ti-6Al-1.2B alloy was investigated in a flowing air over the temperature range 873–1223 K. The alloy exhibited a parabolic oxidation behavior with the activation energy of 250 kJ/mol, which was supposed to be mainly controlled by the inward diffusion of oxygen. The oxide scales consisted mainly of $TiO_2$, a small amount of $Al_2O_3$ and amorphous $B_2O_3$. The morphology of $TiO_2$ changed from fine needle-shape at 1023 K to fine sphere at 1073 K and then well-developed block at a higher temperature. The microstructure of the subsurface showed that $B_2O_3$ pores and crack appear at the Ti/TiB interface above 1023 K as a result of the oxidation of TiB and evaporation $B_2O_3$. Combined with the thermodynamic analysis, it was suggested that the presence of TiB and formation of $B_2O_3$ could not act as an oxidation resistance. Finally, the diffusion coefficient of oxygen in Ti-6Al-1.2B exposure to 1073 K in air was determined to be $4.22 \times 10^{-11}$ $cm^2/s$. 

## 1. Introduction

The application of conventional titanium alloys (e.g., Ti-6Al-4V, wt%) at high temperature is limited by their metastable microstructure, high oxidation rates and loss of strength. Dispersoid strengthening and particle reinforcement of titanium alloy offers the promise of substantial mechanical property improvement at elevated temperature. Dispersoids act as barriers to dislocation motion under condition where thermally activated barriers such as solute atom precipitates and grain boundaries are less effective. In addition, dispersoids refine the microstructure of the matrix alloy and thereby improve the creep and strength properties [1].

Recently, an *in situ* method has been used to prepare titanium matrix alloy [2–5]. TiC [6–8], TiB [3] and $TiB_2$ [9] were widely used as reinforcements because of their similar coefficients of thermal expansion (CTE) and similar densities compared to titanium matrix alloys and their high elastic modulus and strength. Many studies have been performed on the preparation, microstructure and mechanical properties of the *in situ* Ti-based composites. Normally, the formation of *in situ* particles markedly reduces the grain size of the composites, and thus increases the yield strength, ultimate strength and creep properties of composites at room temperature and elevated temperature compared with that of matrix alloy [2, 3, 10, 11]. Because the particles are *in situ* formed in the matrix alloy, no reaction phase has been found at the interface between the TiB and the titanium matrix alloy [12] and only a thin C-diffusion layer was observed at the interface between TiC and Ti-6Al matrix alloy [8]. Also, morphology evolution of *in situ* TiC and TiB in titanium matrix has been investigated in detail [4, 13, 14].

The oxidation of pure titanium has been extensively studied [15]. In the temperature range 1023–1223 K, the oxidation of pure titanium obeys a parabolic rate law followed by a linear region. During the parabolic period the reaction is controlled by the diffusion of the reacting species through a compact $TiO_2$ layer which adheres to the metal. The growth rate of the oxide and the oxygen diffusion coefficient in the substrate and the oxide may be appreciably altered depending on specific alloy's content. However, the oxidation behavior of the *in situ* titanium matrix composites has not been reported so far. So work is needed to assess oxidation behavior of the composites. In this paper, a TiB short fibre reinforced Ti-6Al matrix composite was prepared by an *in situ* method. Isothermal oxidation experiments have been used to reveal the oxidation behavior and oxidation mechanism of *in situ* Ti-based composites.

*On leave from Risoe National Laboratory, Denmark. Now with Department of Mechanical Engineering, Brunel University, Uxbridge UB8 3PH, UK.

TABLE I Chemical composition of the alloys (wt%)

| Alloys | Al | B | O | Ti |
|---|---|---|---|---|
| Ti-6Al-1.2B | 5.33 | 1.15 | 0.22 | Bal. |

## 2. Experimental procedure

### 2.1. Preparation of material

High purity titanium powder (99.7 pct, 45 $\mu$m), aluminum powder (99.6 pct, 29 $\mu$m) and boron powder (99.8pct, <0.5 $\mu$m) were first dry ball milled for 24 hours, then uniaxially pressed into green compacts with 60–70% theoretic density. To prepare composites, the green compacts, pure aluminum and titanium sponge were melted according to the desired composition in a water-cooled copper crucible using a non-consumable tungsten electrode. To ensure chemical homogeneity of the melted alloy, electron magnetic agitation was also used during the melting process and the ingot was melted at least three times. The composition determined by chemical analysis is listed in Table I. Metallographic sample was wet ground with SiC impregnated emery paper using water as the lubricant and subsequently mechanically polished using an alumina-based polishing compound and etched in Kroll's solution. Microstructures were observed on a JEOL 840 scanning electron microscopy (SEM) with energy dispersive spectroscopy (EDS). XRD was performed using Bragg-Brentano geometry with a STOE & CIE $\theta/2\theta$ powder diffractometer equipped with an energy dispersive Kevex detector. The radiation was Cu-$K_\alpha$. Vickers hardness was measured by LEITZ WETZLAR GERMANY 3940 with 100 g load.

### 2.2. Oxidation tests

Oxidation tests were performed in air at a flow rate of 50 $cm^3$/min in the temperature range 873 K to 1223 K for 50 h using a Seiko 320 DTA-TG. The accuracy of 0.01 mg was commonly used in the present study. Oxidation specimens were cut from the ingot and ground to the dimensions of 2.5 mm by 2.5 mm and by 2 mm, followed by mechanical polishing to 6 $\mu$m. They were then ultrasonically cleaned in acetone and water, and dried at 423 K for 1 h before the oxidation tests. A high-purity alumina crucible was used. The specimen was heated to the designated temperature at the rate of 10 K/min and held for 50 h, followed by cooling to room temperature at the rate of 10 K/min. The mass change and the temperature were continuously recorded by a personnel computer. After oxidation, the samples were characterized with respect to the phase constitution by XRD and the microstructure and scale morphology by SEM/EDS. Microhardness was also measured along the cross-section of the metal in order to determine the diffusion coefficient of oxygen.

## 3. Results and analysis

### 3.1. As-received microstructure

Fig. 1 shows the XRD pattern of the as-received Ti-6Al-1.2B alloy. Only the diffraction peaks of TiB and Ti are found and no residual B is found within the sensitivity limits of X-ray diffraction. This implies that TiB has been synthesized as reinforcement through the reaction between Ti and B, and B has been converted into TiB completely.

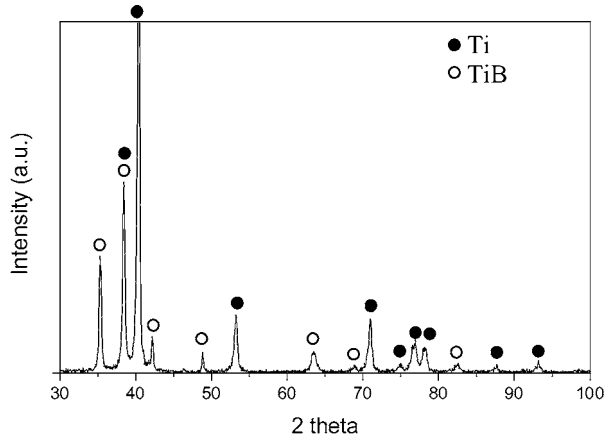


*Figure 1* XRD pattern of the as-received Ti-6Al-1.2B alloy.

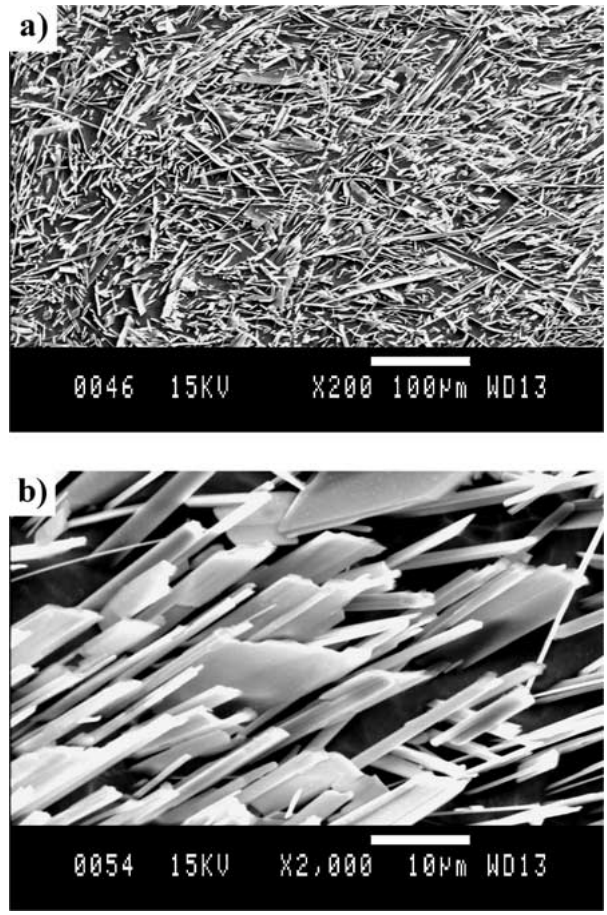


*Figure 2* (a) Microstructure of the as-received Ti-6Al-1.2B alloy, (b) morphology of TiB short fibre, showing rod-shaped and laminar TiB short fibre.

Fig. 2 shows the microstructure of the as-received Ti-6Al-1.2B alloy. In Fig. 2a, TiB with fibrous shape distributes in the matrix homogeneously and isotropically. No special distribution characteristic can be observed. In a higher magnification microstructure, Fig. 2b, TiB is mainly of rod shape with 100–200 $\mu$m in length and 3 $\mu$m in width and the aspect ratio is about

TABLE II Parabolic rate constant at each temperature ($kg^2/m^4 \cdot s$)

| Materials | 873 K | 973 K | 1023 K | 1073 K | 1173 K | 1223 K | 1273 K |
|---|---|---|---|---|---|---|---|
| Ti-6Al-1.2B | $1.59 \times 10^{-11}$ | $3.66 \times 10^{-10}$ | $1.58 \times 10^{-9}$ | $7.52 \times 10^{-9}$ | $9.55 \times 10^{-8}$ | $2.66 \times 10^{-7}$ | |
| $TiO_2$ formation on pure titanium [15] | | | | $1.3 \times 10^{-8}$ | $1.1 \times 10^{-8}$ | | $6.7 \times 10^{-8}$ |

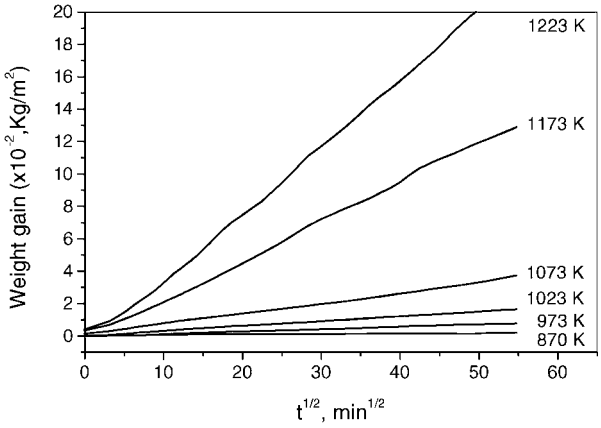


*Figure 3* Weight gain per initial surface area versus the square root of time, for Ti-6Al-1.2B alloy oxidation in air in the temperature range 873–1223 K.

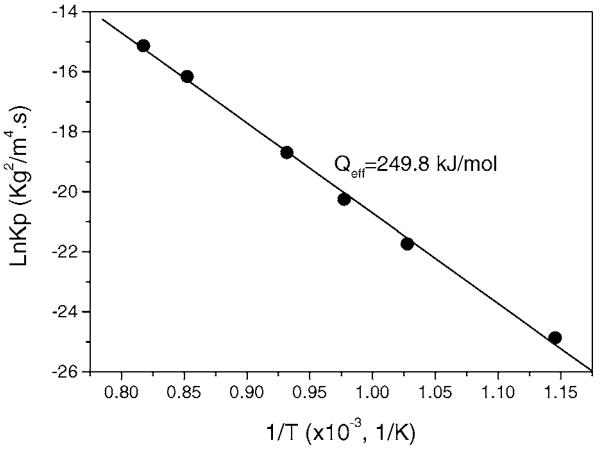


*Figure 4* Arrhenius plot of parabolic rate constant ($k_p$) for oxidation of Ti-6Al-1.2B alloy in flowing air at 50 $cm^3$/min in the temperature range 873–1223 K.

30–70. In addition, some thinner and longer TiB laminae were also observed with 10 $\mu$m or more in width.

## 3.2. Oxidation kinetics

Fig. 3 shows a plot of the weight gain per unit initial surface area versus the square root of the annealing time for Ti-6Al-1.2B in temperature range 873–1223 K. Below 1023 K, the amount of the weight gain is very low. However, the surface of the specimens did show discoloration and the XRD measurement did show the existence of $TiO_2$, indicating that a limited amount of oxidation did occur. Experiment data in Fig. 3 indicate that the oxidation behavior of Ti-6Al-1.2B in 873–1223 K obeys a parabolic rate law.

Usually, the weight gain in titanium alloys is described by a rate equation of the form [16–18]

$$w^n = k_p t \tag{1}$$

where $w$ is the weight gain per unit initial area, $k_p$ the oxidation rate constant, $n$ the rate exponent (=2 for a parabolic oxidation behavior), and $t$ the time. The parabolic rate constant, $k_p$, at each temperature was calculated from the slop of the plot in Fig. 3b and is listed in Table II as well as the value of pure titanium.

Normally, $k_p$ follows an Arrhenius relation of the form

$$k_p = k_0 \exp\left(\frac{-Q_{\text{eff}}}{RT}\right) \tag{2}$$

where $Q_{\text{eff}}$ is the effective activation energy for oxidation, $k_0$ the constant for a given material, $T$ the absolute temperature and $R$ the gas constant. Fig. 4 shows a plot of $\ln k_p$ versus $1/T$. The slop of the plot yields the activation energy of oxidation of Ti-6Al-1.2 alloy to be 250 kJ/mol, slightly less than the value of 267 kJ/mol for Ti-6Al-4V in air in 923–1123 K [19].

## 3.3. Morphology of oxide scale

The specimen surfaces exhibited various colors depending on the oxidation temperature. Oxidation at temperature below 973 K for 50 h resulted in specimen surface discoloration which is blue and gray. In temperature range 1023–1173 K, the specimens were covered by a white layer, which is very brittle and spalls very easily. At 1223 K, the specimen surface was covered by a thick yellow layer.

Fig. 5 shows the X-ray diffraction patterns of the oxide surfaces of Ti-6Al-1.2B alloy oxidized from 973 K to 1223 K for 50 hrs. The standard diffraction pattern of $TiO_2$ was also shown as a reference. At 973 K, the surface mainly consists of Ti, $TiO_2$ and TiB. The presence of Ti and TiB indicates the oxide scale is very thin. It is noted that with the increasing temperature the diffraction intensity of $TiO_2$ increases while that of Ti decreases. This implies that the thickness of the oxide scale increases with the increasing of temperature. At 1223 K, only $TiO_2$ was detected. It must be pointed out that in all oxidized samples no $B_2O_3$ was detected by XRD. But it is well known that TiB oxidizes to $TiO_2$ and $B_2O_3$ according to the following reaction:

$$4/7\,\text{TiB(s)} + \text{O}_2\,\text{(g)} = 4/7\,\text{TiO}_2\,\text{(s)} + 2/7\,\text{B}_2\text{O}_3$$
$$\text{(solid if } T < 723\text{ K, and liquid if } T > 723\text{ K)} \tag{3}$$

Oxidation above 723 K, $B_2O_3$ is liquid but it solidifies during cooling. According to the studies on $B_2O_3$, it was suggested that $B_2O_3$ formed after oxidation was amorphous [19–22], so that it could not be detected by XRD.

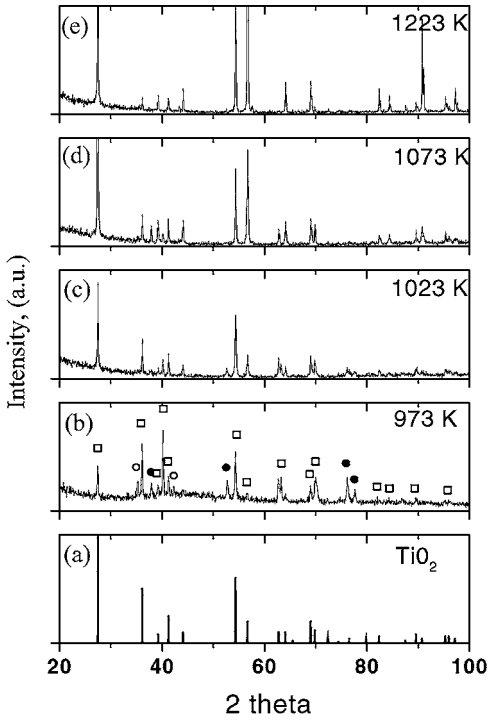


*Figure 5* XRD patterns of the samples surface after 50 h of oxidation in an environment of flowing air at 50 cm$^3$/min at temperatures range 973–1223 K. The standard diffraction peaks of $TiO_2$ is also shown as a reference. (● Ti, ○ TiB, □ $TiO_2$).

Fig. 6 shows the morphologies of the oxide scales formed after oxidation in the temperature range 973–1223 K. At 973 K, Fig. 6a, some bright blocky phases scatter at the surface discontinuously. At 1023 K, a very fine needle-shape phase with 2–3 $\mu$m in length is found as shown in Fig. 6b and c. At 1073 K, a fine spherical phase with about 2 $\mu$m in diameter was formed (Fig. 6d). At 1223 K, a well-developed and regularly blocky phase with about 10–50 $\mu$m in length can be clearly observed from Fig. 6e. All these phases were confirmed by EDS to be titanium oxide. According to the XRD results shown in Fig. 5, it can be concluded that the oxide is $TiO_2$. However, no $Al_2O_3$ and $B_2O_3$were detected by XRD and identified by EDS. Except for the amorphous $B_2O_3$, another reason may be due to that the amount of $Al_2O_3$ and $B_2O_3$ is too small to be detected.

### 3.4. Microstructure of the subsurface

Fig. 7a and b show the microstructure of the subsurface after oxidation at 873 K and 973 K for 50 hr, respectively. The oxide scales are 2 $\mu$m in thickness at 873 K and 5 $\mu$m at 973 K. Compared with the microstructure before oxidation, no significant difference can be observed in both the morphology of TiB and the microstructure of Ti-6Al matrix alloy.

At 1023 K, some pores appear in the subsurface to lead to a porous oxide scale, which is about 10–15 $\mu$m in thickness, as shown in Fig. 8a. It is noticed from Fig. 8a and b that within and below the porous oxide scale some pores are found at the interface between TiB fiber and the matrix. As the temperature increases to 1073 K, while the porous layer increase to about 20–30 $\mu$m in thickness, cracks also appear in this oxide scale to form a stratified oxide scale (Fig. 9a). In addition, more pores are found at the Ti/TiB interface and some of them are connected each other to form a crack along the Ti/TiB interface, as shown in Fig. 9b. It must be pointed out in the entire oxide scale TiB fibers are still seen clearly.

At 1173 K, a oxide layer that consists of a relatively dense layer and a porous layer is observed in Fig. 10a. In the porous layer, Fig. 10b, the pores are observed not only at the Ti/TiB interface but also within the matrix. The relatively dense layer in fact is still porous, but no TiB fibers can be seen any longer (Fig. 10c). When the temperature is up to 1223 K, almost a similar microstructure is observed.

## 4. Discussion

### 4.1. Thermodynamics

From above results, the main oxidation reactions involved in the present case are

$$\mathrm{Ti\,(s)} + \mathrm{O_2\,(g)} = \mathrm{TiO_2\,(s)} \tag{4.1}$$

$$4/7\,\mathrm{TiB\,(s)} + \mathrm{O_2(g)} = 4/7\,\mathrm{TiO_2(s)} + 2/7\mathrm{B_2O_3} \times(\mathrm{s\ or\ l,\ amorph.}) \tag{4.2}$$

here (s), (l), (g) and (amorph) refer to the solid, liquid, gaseous and amorphous states, respectively.

The Gibbs free energy for the above reactions can be written respectively as

$$\Delta G_1 = \Delta G_1^o + RT \ln \frac{a_{\mathrm{TiO_2}}}{a_{\mathrm{Ti}} P_{\mathrm{O_2}}} \tag{5.1}$$

for the reaction (4.1), and

$$\Delta G_2 = \Delta G_2^o + RT \ln \frac{a_{\mathrm{TiO_2}}^{4/7} a_{\mathrm{B_2O_3}}^{2/7}}{a_{\mathrm{TiB}}^{4/7} P_{\mathrm{O_2}}} \tag{5.2}$$

for the reaction (4.2), where $P_{\mathrm{O_2}}$ is the partial pressure of oxygen in the oxidation environment; $\alpha$ the activity and $\Delta G^o$ the standard Gibbs free energy which can be represented as

$$\Delta G^o = \sum \Delta G^o(\mathrm{products}) - \sum \Delta G^o(\mathrm{reac\,tan\,}ts) \tag{6}$$

For TiB, TiO and $B_2O_3$, the activities are assumed to be unity. For the Ti, the activity is also assumed to be unity because the molar fraction of Ti in the composite is very high. So the Gibbs free energy can be rewritten as

$$\Delta G_1 = \Delta G_1^o + RT \ln \frac{1}{P_{\mathrm{O_2}}} \tag{7.1}$$

$$\Delta G_2 = \Delta G_2^o + RT \ln \frac{1}{P_{\mathrm{O_2}}} \tag{7.2}$$

We consider the oxidation environment in present as an ideal gas mixture, so the partial pressure of oxygen is

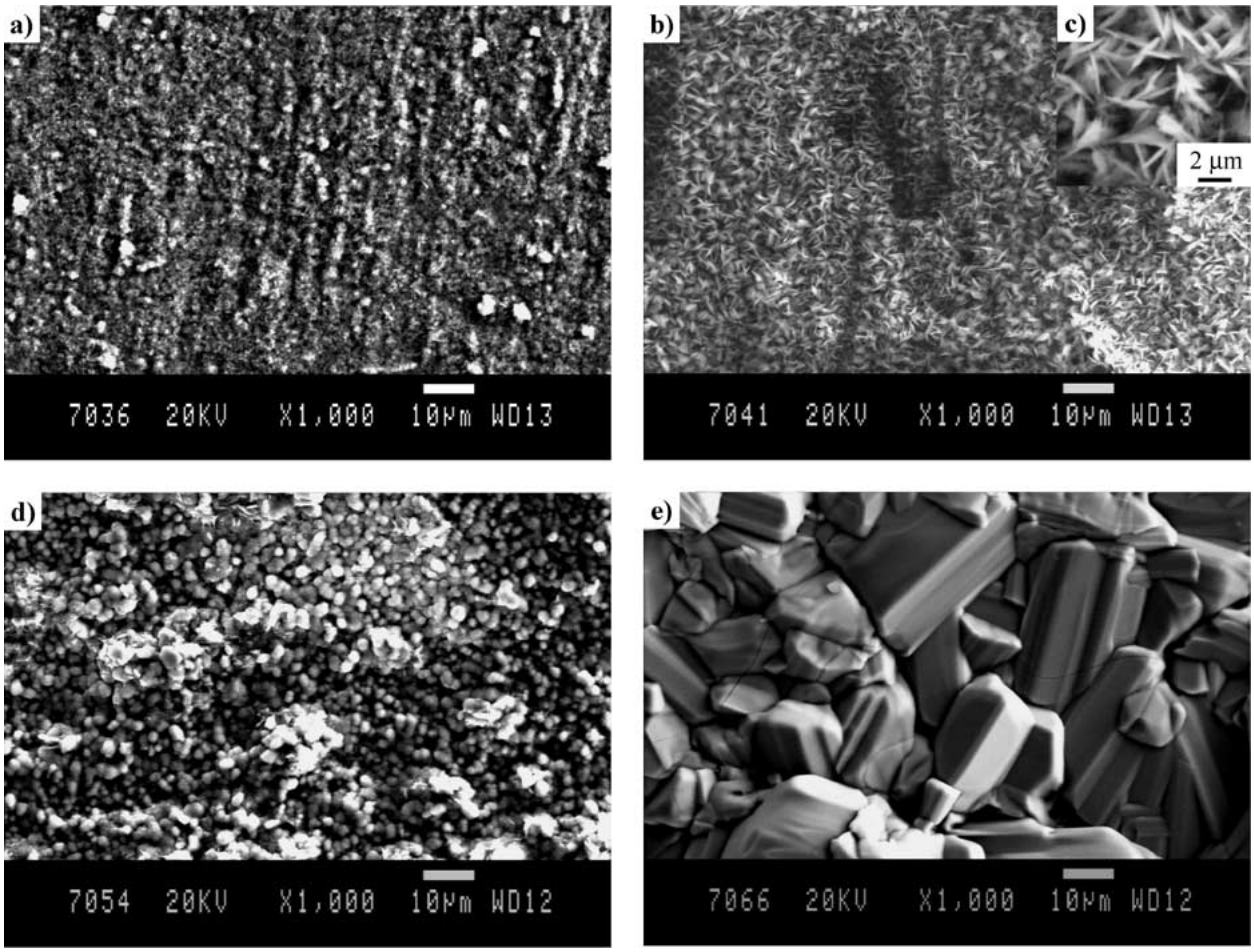


*Figure 6* Surface morphology of oxide scale formed after 50 h of oxidation in an environment of flowing air at 50 $cm^3$/min at temperatures range 973–1223 K. (a) 973 K, (b) and (c) 1023 K, (d) 1073 K, (e) 1223 K.

TABLE III Thermodynamic data of TiB, Ti, $O_2$,$TiO_2$ and $B_2O_3$ [23]

| | $G^o$ (kJ/mol) | | | | |
|---|---|---|---|---|---|
| $T$ (K) | Ti | $O_2$ | $TiO_2$ | TiB | $B_2O_3$ |
| 600 | −21.47 | −126.60 | −980.02 | −185.60 | −1308.10 |
| 800 | −32.19 | −172.88 | −1002.77 | −199.75 | −1339.24 |
| 1000 | −44.44 | −220.83 | −1027.07 | −216.45 | −1377.08 |
| 1200 | −54.85 | −270.15 | −1054.32 | −235.24 | −1420.21 |

given by

$$P_{O_2} = x_{O_2} P \approx 0.21 \text{ atm} = 21278.25 \text{ Pa} \quad (8)$$

where $x_{O_2}$ is the molar fraction of $O_2$ in the air and $P$ is the total pressure of the oxidation environment.

The standard Gibbs free energy data for Ti, TiB, $O_2$, $TiO_2$ and $B_2O_3$ are listed in Table III. Fig. 11 shows the calculated results of Gibbs free energy for the reactions in the temperature range 600–1200 K. First from the figure, it was found that the Gibbs free energys are negative in the whole research temperature range (873–1173 K), indicating that these two reactions will happen thermodynamically. Second, the Gibbs free energy for the reaction (4.1) is obviously lower than that for the reaction (4.2), which displays that the reaction (4.1) has thermodynamic priority to happen. It has been pointed out before that the melting point of $B_2O_3$ is about 723 K, which means that during the present oxidation process the $B_2O_3$ was in liquid. It was well known that diffusion in liquid is much faster than that in solid. In addition, when the temperature is over 1023 K, the $B_2O_3$ begins to evaporate (it will be discussed in the next paragraph), which will break the reaction balance in the reaction (4.2) and accelerates the reaction rate. So from the point of view of thermodynamics and the state of the oxide scale, it was strongly suggested that the formation of $B_2O_3$ could not act as an oxidation resistance and the existence of TiB could not improve the oxidation resistance.

## 4.2. Formation of pores and the crack

From the microstructures of the subsurface, it was found that the pores appear first at the Ti/TiB interface at about 1023 K. With the increasing of temperature more pores appear at the Ti/TiB interface and within the matrix. It was reported that $B_2O_3$ begins to evaporate considerably at 1073 K [19] and extensively about 1273 K [24, 25]. The evaporating temperature, 1073 K, is very close to the temperature for which the pores appear at the Ti/TiB interface in the present case. The fact that more pores appear at the interface and within the matrix above 1073 K is also in good agreement with the extensive evaporation of $B_2O_3$ above 1073 K. From these it was concluded that the pores observed at the interface are $B_2O_3$ gas pores.

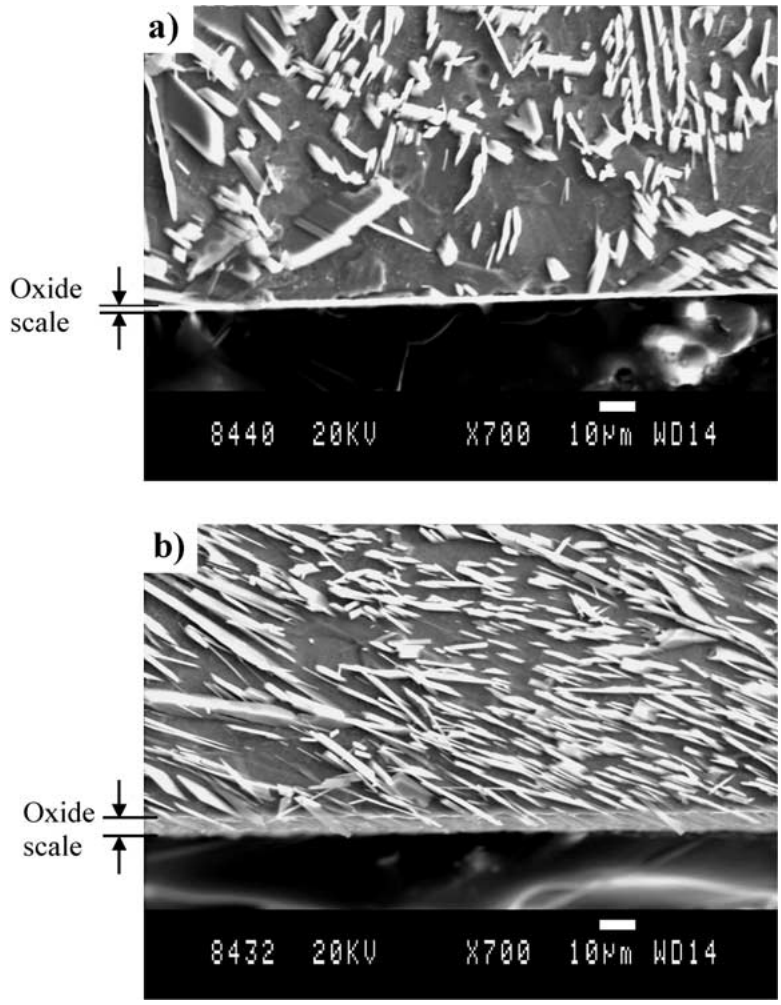


*Figure 7* Cross-sectional microstructure formed after oxidation for 50 h at (a) 873 K and (b) 973 K.

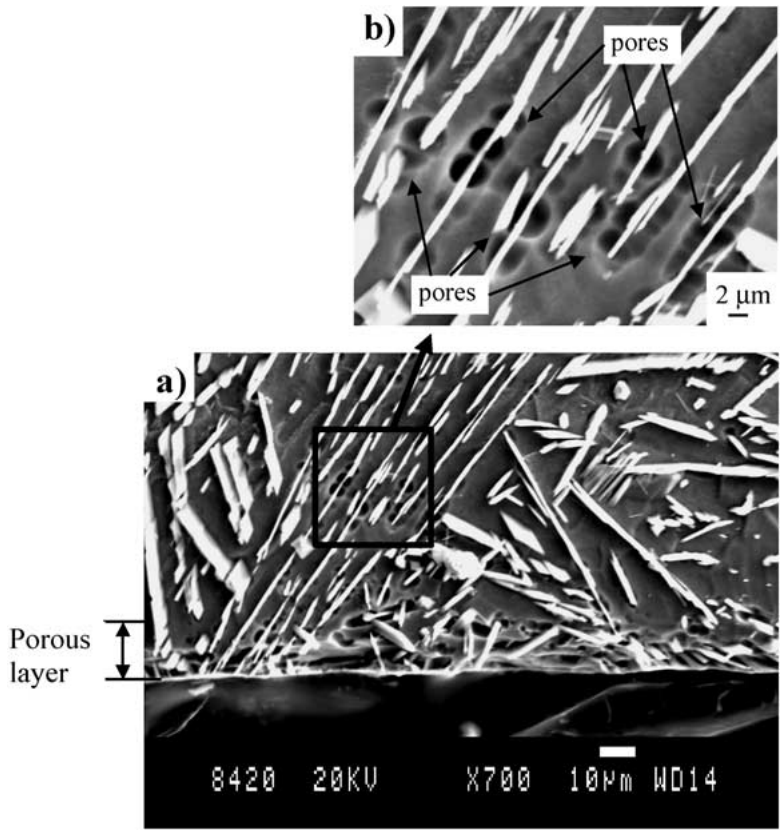


*Figure 8* Cross-sectional microstructure of the subsurface formed after oxidation for 50 h at 1023 K, (a) porous oxide scale, (b) pores formed at the interface between TiB fibre and matrix.

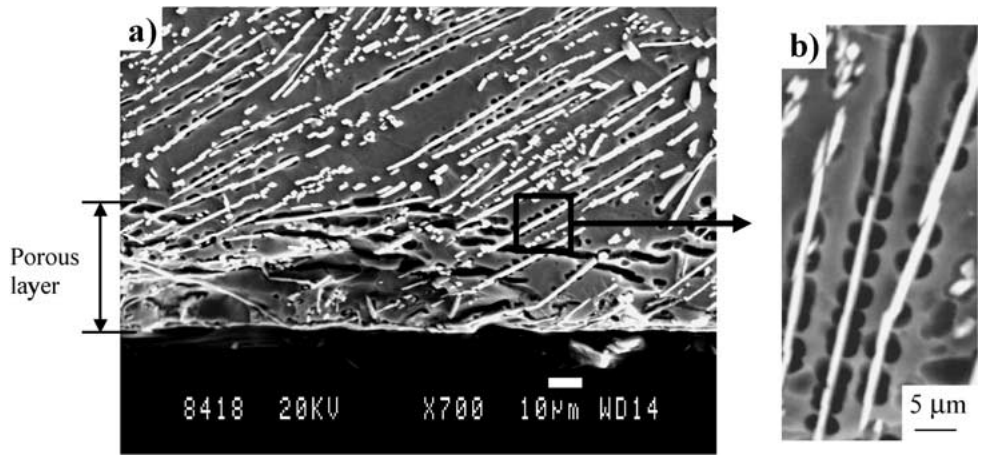


*Figure 9* Cross-sectional microstructure of the subsurface formed after oxidation for 50 h at 1073 K, (a) stratified oxide scale, (b) pores at the interface between TiB and matrix.

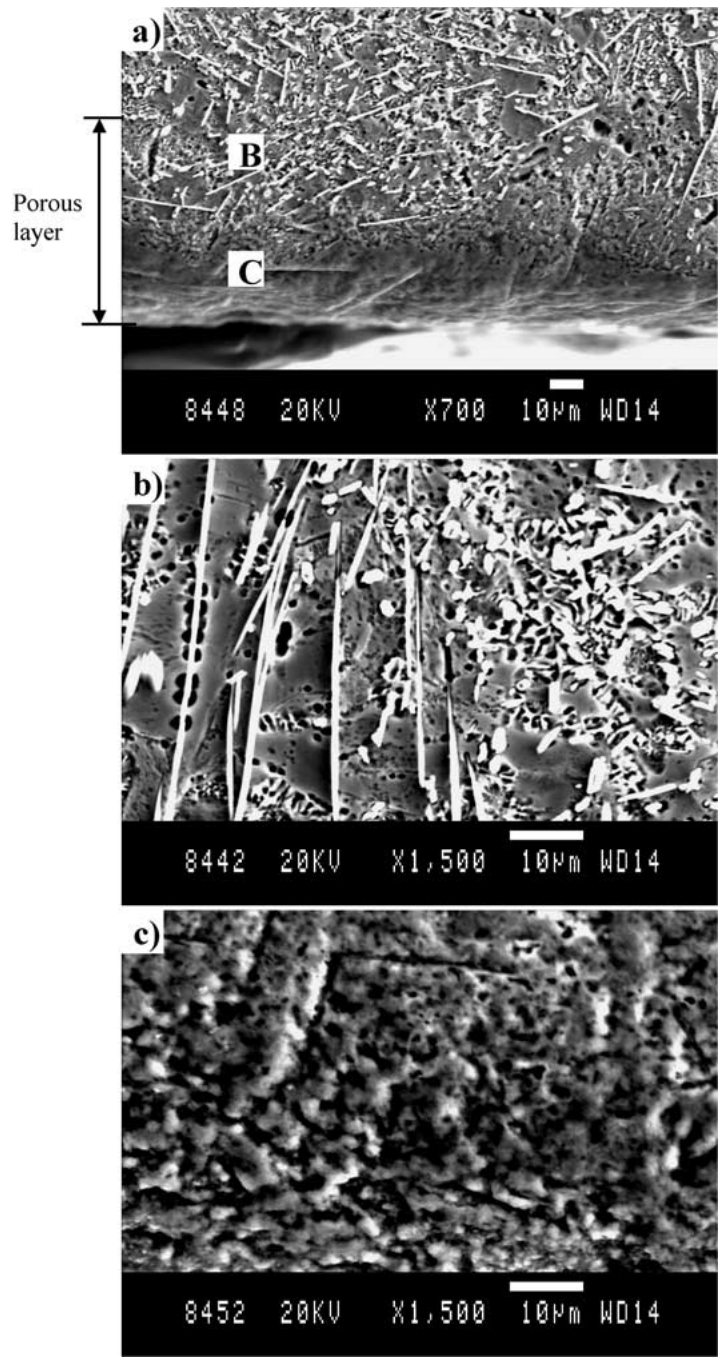


*Figure 10* (a) Cross-sectional microstructure of the metal formed after oxidation for 50 h at 1173 K, (b) microstructure of part B marked in Fig. 10a, (c) microstructure of the porous oxide scale, marked as C in Fig. 10a.

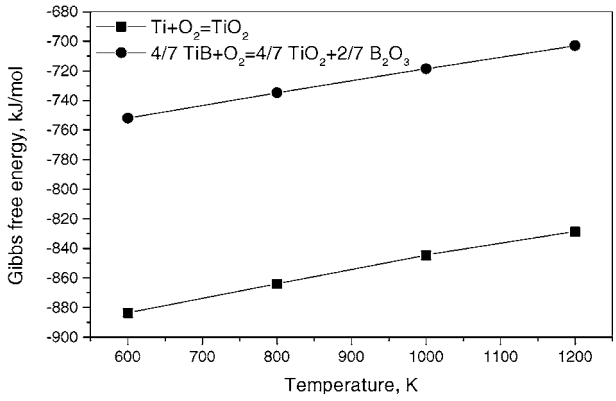


*Figure 11* The change of the Gibbs free energy versus temperature.

Also from the subsurface microstructure results, the formation of pores and the crack during the oxidation can be summarized as following:

1. The reaction between $O_2$ and TiB happens through the reaction (3) at the Ti/TiB interface for some reasons, such as the poor wettability of the titanium melting to TiB ceramic fiber and the difference between the thermal expansion coefficients of TiB ($8.6 \times 10^{-6}$ 1/K) and titanium ($9.6 \times 10^{-6}$ 1/K) that results in the faster diffusion of oxygen along the Ti/TiB interface.
2. As the temperature increases to about 1023 K, the $B_2O_3$ begins to evaporate and $B_2O_3$ gas pore appears at the end of TiB fiber or someplace at the Ti/TiB interface, as shown in Fig. 12a. Then a crack tip is formed at the interface, marked in Fig. 12b.

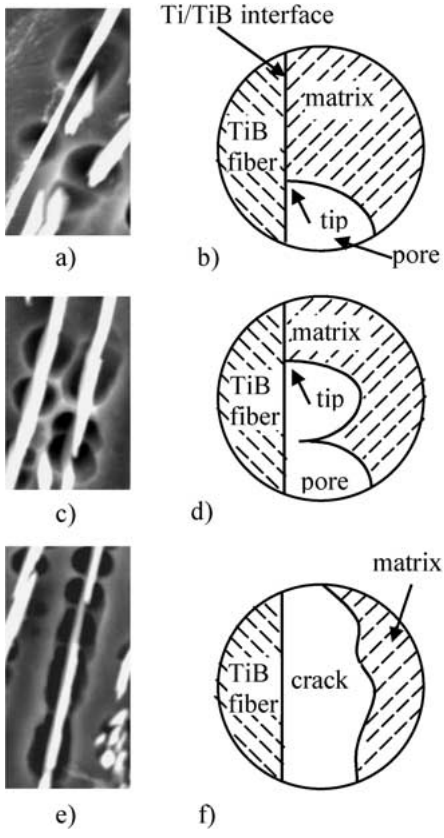


*Figure 12* Schematic of the formation of pores and the crack at the Ti/TiB interface.

3. With the increasing of oxidation time or temperature, another pore appears just ahead of the last pore through the crack tip (Fig. 12c) and the crack tip propagates forward (Fig. 12d).
4. Finally, a crack is formed along the Ti/TiB interface as a result of the oxidation of TiB and the propagating of the crack tip, shown in Fig. 12e and f. So the oxidation process happened at the Ti/TiB interface is in fact a crack propagation process.

It must be pointed out that the appearance of pores and cracks along the Ti/TiB interface suggested that the oxidation of TiB might reduce the oxidation resistance of Ti-6Al-1.2B because the cracks and pores can be an easy diffusion path of oxygen.

### 4.3. Supposed oxidation mechanism

The weight gain of Ti-6Al-1.2B alloy in Fig. 3 indicated that oxidation process obeys a parabolic rate law. This means that the oxidation process is controlled by the diffusion of the active species through the oxide scale. The calculated oxidation activation energy of Ti-6Al-1.2B, 250 kJ/mol in the temperature range 873–1223 K, is quite close to the activation energy for diffusion of both oxygen and titanium in $TiO_2$, 234 kJ/mol and 257 kJ/mol, [21] respectively. This suggests that both the outward diffusion of titanium and the inward diffusion of oxygen through the oxide scale might exist. From the microstructure of the subsurface oxidized at 1073 K for 50 hrs, it was found that there still exist a lot of TiB fibers in the surface of the oxide scale layer (Fig. 9a). This result strongly indicates that the oxide scale mainly grows inward. In other words, the oxidation process is mainly controlled by the inward oxygen diffusion.

### 4.4. Determination of diffusion coefficient of oxygen

The microhardness technique is a convenient method to determine diffusion properties of dissolved species in metallic matrix. In addition, from the microhardness data the amount of dissolved oxygen can also be determined [26]. In order to determine the diffusion coefficient of oxygen in titanium alloy, a model is briefly described. At first, following assumptions were made:

1. Ti-6Al-1.2B alloy is a one-phase material so that only one diffusion coefficient of oxygen will be considered in the following calculation.
2. A constant diffusion coefficient is independent of the oxygen concentration.
3. The specimen is considered as a semi-infinite one-dimensional system.

Then, the diffusion of oxygen from the interface between oxide scale and metal ($d = 0$) into the one-phase Ti-6Al-1.2B alloy (one dimensional version) can be described by Fick's second law

$$\frac{\partial C}{\partial t} = D\frac{\partial^2 C}{\partial d^2} \tag{9}$$

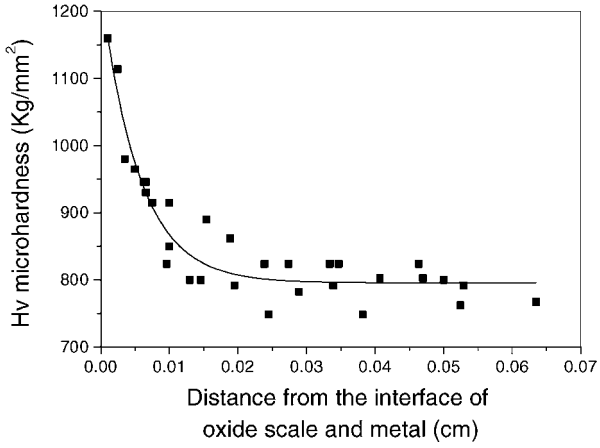


*Figure 13* Microhardness of Ti-6Al-1.2B alloy along the cross-section after oxidation at 1073 K in air for 50 h and the fitting curve (solid line).

where $C = (d, t)$is the concentration of the oxygen at the distance $d$ from the interface after a certain time $t$. The solution of this equation, on the basis of assumption of diffusion in one-dimensional from a infinite source at $d = 0$ into a semi-infinite material, is given by the relationship

$$\frac{(C - C_s)}{(C_0 - C_s)} = erf\left(\frac{d}{2\sqrt{Dt}}\right) \tag{10}$$

where $C_0$ is the initial concentration of the oxygen in Ti alloy $[C_0 = C(d, t = 0)]$, $C_s$ the concentration at the interface $[C_s = C(d = 0, t)]$ and $D$ is the diffusion coefficient of oxygen. More studies [21–22] have shown that a linear relationship between the microhardness of the material and the concentration of dissolved species can be considered. Consequently, the above equation can be rewritten by

$$H = H_s + (H_o - H_s)\, erf\left(\frac{d}{2\sqrt{Dt}}\right) \tag{11}$$

where $H$ is the microhardness. $H_0$ is the initial microhardness of the materials $(C = C_0)$ and $H_s$the microhardness at the interface $(C = C_s)$.

Fig. 13 shows the microhardness of the Ti-6Al-1.2B alloy after oxidation at 1073 K for 50 h. Fitting Equation 11 to the experimental data, as shown in Fig. 13 as the solid line, the diffusion coefficient of oxygen in Ti-6Al-1.2B alloy was determined to be $4.22 \times 10^{-11}$ cm$^2$/s. This value is in good agreement with the value of David *et al.* [27] in titanium alloy, i.e., $8.4 \times 10^{-11}$ cm$^2$/s.

## 5. Conclusion

1. The oxidation behavior of *in situ* TiB short fibre reinforced Ti-6Al-1.2B alloy in air in the temperature range 873–1223 K obeys the parabolic law with an activation energy of 250 kJ/mol, which was supposed to be mainly controlled by the inward diffusion of oxygen.

2. Because of the oxidation of TiB and evaporation of $B_2O_3$, $B_2O_3$gaspores appear at the Ti/TiB interface above 1023 K, which leads to the formation of the crack along the interface.

3. The thermodynamic analyses and the microstructure results indicate that the presence of TiB in Ti-6Al-1.2B alloy can not act as an oxidation resistance.

4. The diffusion coefficient of oxygen in Ti-6Al-1.2B was calculated to be $4.22 \times 10^{-11}$ cm$^2$/s at 1073 K.


## Acknowledgement

One of the authors (Erlin Zhang) is grateful to Mr. John Kjøller at Materials Research Department of Risø National laboratory, Denmark, for the DAT experiment. This work is partly supported by the Foundation of National Key Lab. for Precision Hot Processing of Metal, Harbin Institute of Technology of China. (Contract No. 99JS61.5.1.ZS6102).


## References


1. S. J. SHU, S. MUKHERJI, W. CHEN, Y. X. LU, Z. G. WANG and R. P. WAHI, *Mat. Sci. Eng. A-Struct.* A **256** (1998) 301.
2. H. T. TSANG, C. G. CHAO and C. Y. MA, *Scripta Mater.* **37**(9) (1997) 1359.
3. T. YAMAMOTO, A. OTSUKI, K. ISHIHARA and P. H. SHIGN, *Mat. Sci. Eng. A-Struct.* A **239/240** (1997) 647.
4. S. S. SAHAY, K. S. RAVICHANDRAN, R. AFRI, B. CHEN and J. RUBIN, *J. Mater. Res.* **14**(11) (1999) 4214.
5. S. C. TJONG and Z. Y. MA, *Mat. Sci. Eng. A-Struct.* **29R** (2000) 49.
6. B YANG, E. L. ZHANG, Y. X. JIN and S. Y. ZENG, *J. Mater. Sci. Technol.* **17**(1) (2001) 103.
7. ERLIN ZHANG, YUNXUE JIN, SONGYAN ZENG and ZHAOJUN ZHU, *J. Mater. Sci. Lett.* **20**(11) (2001) 1063.
8. ERLIN ZHANG, SONGYAN ZENG and ZHAOJUN ZHU, *J. Mater. Sci.* **35**(23) (2000) 5989.
9. L. LU., M. O. LAI and Y. WANG, *ibid.* **35** (2000) 241.
10. Z. Y. MA, S. C. TJONG and L. GEN, *Scripta Mater.* **42** (2000) 367.
11. W. O. SOBOYEJO, R. J. LEDERICH and S. M. L. SASTRY, *Acta. Mater.* **42**(8) (1994) 2579.
12. D. X. LI, D. H. PING, Y. X. LU and H. Q. HE, *Mater Lett.* **16**(6) (1993) 322.
13. M. E. HYMAN, C. McCULLOUGH, J. J. VADENCIA, C. G. LEVI and R. MEHRABIAN, *Metall. Mater. Trans.* A **20A**(9)(1989)1847.
14. M. E. HYMAN, C. McCULLOUGH, C. G. LEVI and R. MEHRABIAN, *ibid.* **27A**(7) (1991) 1647.
15. P. KOFSTADT, "High Temperature Oxidation of Metal" (Wiley, New York, 1966).
16. E. LEE and J. WALDMAN, *Scripta Metall.* **22** (1988) 1389.
17. R. SHENOY, J. UNNAM and R. CLARK, *Oxid. Met.* **26** (1986) 105.
18. A.-M. CHAZE, C. CODDETT and G. BERANGER, *J. Less-common Metal* **83** (1982) 49.
19. H. L. DU, P. K. DATTA, D. B. LEWIS and J. S. BURNELL-GRAY, *Corrosion Science* **36** (1994) 631.
20. T. GRAZIANI, E. LANDI and A. BELLOSI, *J. Mater. Sci. Lett.* **12** (1993) 691.
21. B. G. VELASCO and P. B. ASWATH, *J. Mater. Sci.* **33** (1998) 2203.
22. K. SUZUKI, K. NISHIKAWA and S. WATAKABE, *Materials Transaction JIM* **38**(1) (1997) 54.
23. D. L. YE (ed.), "Handbook of Thermodynamic Data of Inorganic Compounds" (Metallurgical Industry Press, Beijing, 1988).
24. V. B. VOITOVICH, V. A. LARRENKO and V. M. ADEJEV, *Oxid. Met.* **42** (1994) 145.
25. M. G. BARANDIKA, J. J. ECHEBERRIA, J. M. SANCHEZ and F. CASTRO, *J. Mater. Chem.* **8** (1998) 1851.
26. B. COCKERAM and R. A. RAPP, *Oxid. Met.* **45** (1996) 427.
27. D. DAVID, G. BERANGER and E. A. GARCIA, *J. Electrochem. Soc.* **130**(2) (1983) 1423.



*Received 21 January*
*and accepted 22 May 2002*